Available online at www.sciencedirect.com

ScienceDirect

Procedia Computer Science 126 (2018) 244–253

Procedia Computer Science

www.elsevier.com/locate/procedia

International Conference on Knowledge Based and Intelligent Information and Engineering Systems, KES2018, 3-5 September 2018, Belgrade, Serbia

Automatic Characterization of the Serous Retinal Detachment Associated with the Subretinal Fluid Presence in Optical Coherence Tomography Images

Joaquim de Moura[a,b,*], Jorge Novo[a,b], Susana Penas[c], Marcos Ortega[a,b], Jorge Silva[d,f], Ana Maria Mendonça[e,f]

[a] *Faculty of Informatics, Department of Computing, University of A Coruña, A Coruña, Spain*
[b] *CITIC-Research Center of Information and Communication Technologies, University of A Coruña, A Coruña, Spain*
[c] *Department of Ophthalmology, São João Hospital Centre, Porto, Portugal*
[d] *Faculty of Engineering, Department of Informatics Engineering, University of Porto, Porto, Portugal*
[e] *Faculty of Engineering, Department of Electrical and Computer Engineering, University of Porto, Porto, Portugal*
[f] *INESC-TEC, Porto, Portugal*

Abstract

An accurate detection of the macular edema (ME) presence constitutes a crucial ophthalmological issue as it provides useful information for the identification, diagnosis and treatment of different relevant ocular and systemic diseases. Serous Retinal Detachment (SRD) is a particular type of ME, which is characterized by the leakage of fluid that has a propensity of being accumulated in the macular region. This paper proposes a new methodology for the automatic identification and characterization of the SRD edema using Optical Coherence Tomography (OCT) images. The subretinal fluids and the External Limiting Membrane (ELM) retinal layers are identified and characterized to measure the disease severity. Four different visualization modules were designed including representative derived parameters to facilitate the doctor's work in the diagnostic evaluation of ME. The different steps of this method were validated using the manual labelling provided by an expert clinician. The validation of the proposed method offered satisfactory results, constituting a suitable scenario with intuitive visual representations that also include different relevant biomarkers.

Keywords: Computer-aided diagnosis; optical coherence tomography; diabetic macular edema; serous retinal detachment

1. Introduction

In 2015, diabetes was directly responsible of 1.6 million deaths worldwide. Also, the number of people with this disease is predicted to be estimated over 200 million people by the year 2025, according to the data of the World Health Organization (WHO) guidelines [1]. Diabetes may lead to significant complications in many parts of the body, affecting

* Corresponding author. Tel.: +34-881011330; fax: +34-981167160.
E-mail address: joaquim.demoura@udc.es

10.1016/j.procs.2018.07.258

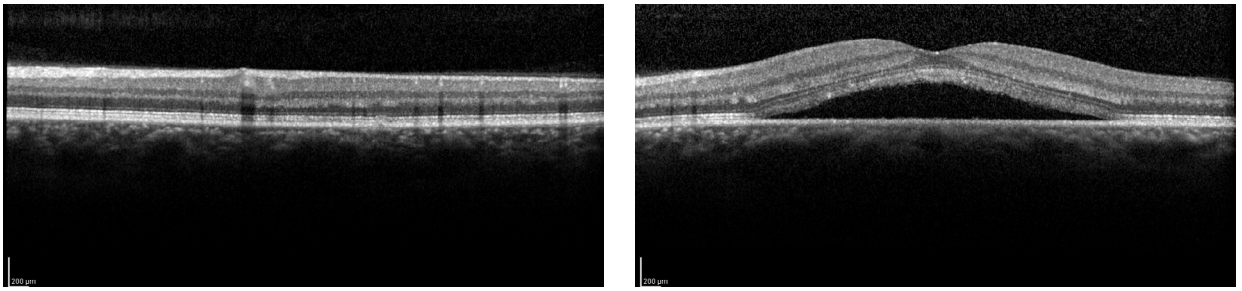

(a) (b)

Fig. 1. Representative examples of OCT retinal images. (a) OCT image without SRD edema. (b) OCT image with the presence of a SRD edema.

the circulatory system and damaging the blood vessels[2]. This may provoke severe macrovascular and microvascular damages that could derive in a heart attack, stroke, insufficiency in blood flow to legs, kidney failure (nephropathy), nerve damage (neuropathy) or vision loss (diabetic retinopathy)[3].

Diabetic Retinopathy (DR) and Macular Edema (ME) constitute serious eye conditions that are caused mainly by the abnormal formation of the retinal microvasculature that is associated with a prolonged hyperglycemia of the diabetes mellitus. They represent the leading causes of preventable blindness in the working-age population of developed countries, representing a serious public health problem[4]. In particular, ME is defined as a focal or diffuse retinal thickening derived by the intraretinal fluid accumulation in the macula, which is the central region of the retina where the vision is most acute[5]. This fluid accumulation can generate an abnormal change in the morphology of the retinal tissues that is characterized mainly by an elevation or rupture of the External Limiting Membrane (ELM) retinal layer[6]. If this disease is not diagnosed or treated appropriately, it could lead to an irreversible damage to the macular region, resulting in the progressive loss of the central vision.

Currently, the diagnosis and monitoring of the ME disease is mostly performed through the visual analysis of Optical Coherence Tomography (OCT) images[7]. OCT is a non-invasive imaging modality that is capable of providing high-resolution cross-sectional images of the neurosensorial retina in real time with micron-level resolution[8]. Otani *et al.*[9] proposed a clinical classification of the ME disease in three different types based on the presence of visible morphological patterns of the intraretinal fluid accumulation in OCT images. These types of ME are clinically defined as: Serous Retinal Detachment (SRD), Diffuse Retinal Thickening (DRT) and Cystoid Macular Edema (CME). This clinical classification was posteriorly expanded in the work of Panozzo *et al.*[10], classifying in these same three types of ME but using additional different criteria, such as retinal thickness, diffusion, volume, morphology or the vitreous traction[11]. In this work, we focus on a specific clinical type of ME, the SRD edema. This edema is characterized by the leakage of fluid under the retina that has a propensity of being accumulated in the space between the Inner Limiting Membrane (ILM) and the Retinal Pigment Epithelium (RPE) layer. This fluid accumulation may lead to permanent macular damages as, for example, the retinal detachment or the progressive loss of the central vision[12]. Fig. 1 shows representative examples of OCT images with and without the presence of the SRD edema.

Over the last years, some proposals were presented related to the ME analysis using the OCT images as source of information. As reference, Lee *et al.*[13] proposed an automatic classification of the pigment epithelial detachments into three categories: serous, drusenoid and fibrovascular. This system was based on the mean internal intensity and the standard deviation of the internal intensity in each individual OCT scan. Hassan *et al.*[14] employed a Support Vector Machine (SVM) classifier based on five distinct features (three based on the thickness profiles of the sub-retinal layers and two based on cyst fluids within the sub-retinal layers) for the detection of the SRD edema. Wu *et al.*[15] proposed a continuous max flow approach using a probability map after training samples using the random forest classification for the SRD segmentation and the pigment epithelial detachment. A different strategy by Schlegl *et al.*[16], as the authors presented a method based on deep learning and a 3D region growing process for the extraction of the macular fluid accumulations in retinal images. Samagaio *et al.*[17] proposed the localization of the three types of ME in OCT images. In this work, specific strategies using image processing and machine learning methods were applied to identify the presence of each ME type.

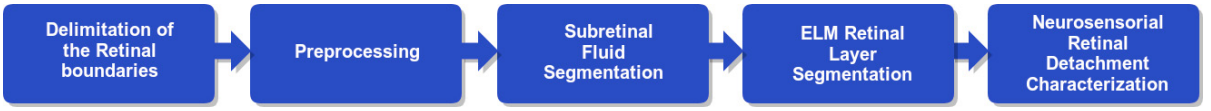

Fig. 2. Main steps of the proposed methodology.

Most of the computational methodologies were proposed to generally detect the macular fluid in an automated manner using OCT images. However, these systems are limited only to detect the fluid presence or absence without practically addressing the problem of the complete quantification and characterization of SRD edemas jointly with the subsequent elevation and detachment of the retinal layers. In this way, this work presents the development of a novel and complete methodology for the automatic detection, quantification and characterization of the SRD edema associated with the subretinal fluid presence in OCT images, following the clinical classification of international reference in the ophthalmological field[9 10]. In order to achieve this, different complementary image processing techniques were combined to identify and extract the subretinal fluids and the ELM layer. Then, using this identifications as source of information, the system provides different visualization modules as well as representative derived biomarkers to facilitate the posterior analysis of the SRD edema by the expert clinician.

This paper is organized as follows: Section 2 describes the characteristics of the implemented methodology. Results and discussions are presented and discussed in Section 3. Finally, Section 4 shows the conclusions as well as possible future lines of work.

2. Methodology

The proposed methodology is divided into five main steps: a first step, where the boundaries of the retina are delimited; second, a preprocessing is applied to eliminate noise and enhance the main characteristics of the SRD edema; third, the subretinal fluid is identified and segmented; fourth, the elevation and detachment of the retinal layers are identified; and a final fifth step, where we analyse the SRD edema through different visualization modules and complementary derived biomarkers that provide an intuitive way of quantification and characterization of this type of edema to be analysed by specialist. Each one of these steps is going to be discussed next. A schematic representation of the main steps of this methodology can be seen in Fig. 2.

2.1. Delimitation of the Retinal Boundaries

The proposed method takes, as input, an OCT image. This image corresponds to the histological appearance of the retinal structure in the macular region. Two retinal layers were identified as they delimit the retinal boundaries, region where the SRD edemas typically appear. These two retinal layers are the ILM and RPE. For this purpose, we used an approach based on the work of Chiu *et al.*[18], where the retinal layers are segmented using a graph theory and dynamic programming approach. Firstly, the method calculates the intensity gradients in order to identify the retinal layers. Then, these gradients are used as weights in the search of the minimum weighted paths using the Dijkstra algorithm[19]. In Fig. 3, we can see a representative example of this step where the ILM and RPE layers were segmented.

2.2. Preprocessing

OCT images are often affected by motion artefacts, speckle noise or poor soft tissue contrast, complicating enormously the analysis of the retinal structures and pathologies. In this way, we designed a preprocessing stage applying a sequence of some well-known filters in order to eliminate the noise and small artefacts, in addition to increase the contrast of structures of interest, as the aimed subretinal fluid region.

Fig. 4 includes an example of application of the steps of this preprocessing stage. Firstly, we use an anisotropic diffusion filtering to remove noise, also preserving and improving the structure of the edges (Fig. 4(b)). This method is based on the principle of discretization schemes of the anisotropic diffusion tensor. The direction and magnitude of diffusion were estimated and correlated[20]. Then, we apply an adaptive compensation filter to attenuate the shadows of

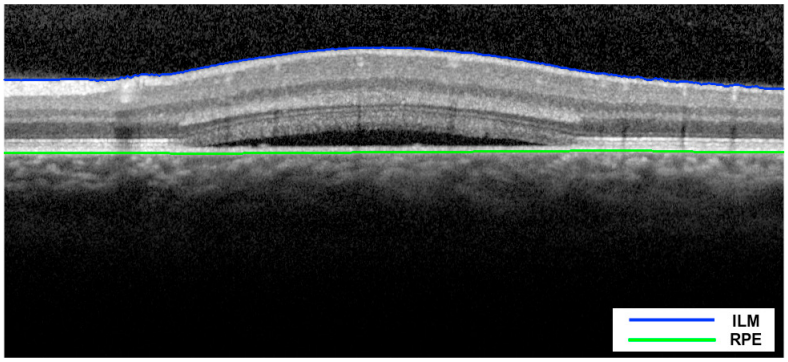

Fig. 3. Example of ILM and RPE retinal layer segmentation.

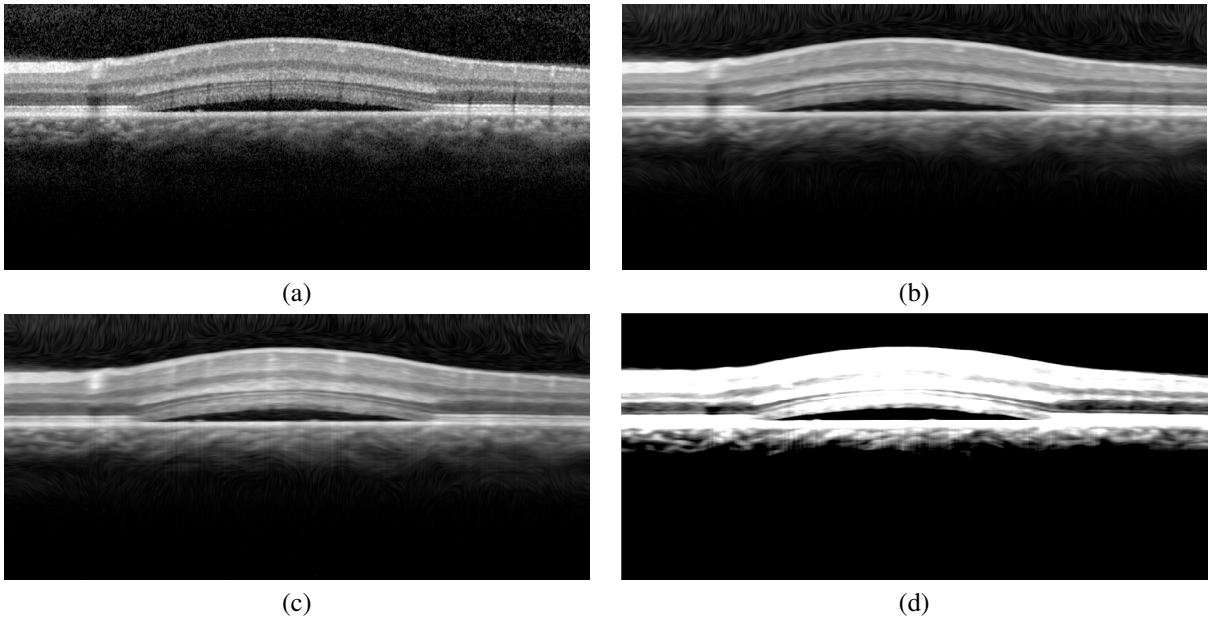

Fig. 4. Example of the preprocessing stage. (a) Input image. (b) Preprocessed image after applying the anisotropic diffusion filter. (c) Preprocessed image after applying the adaptive compensation filter. (d) Preprocessed image after the adjustment of the intensity values.

the retinal vessels and improve the contrast between the subretinal fluids and the normal tissues (Fig. 4(c)). This filter removes the vessel shadows by several consecutive standard compensation operations. Its application is iteratively applied until an energy threshold is reached, when the compensation process is stopped. This way, we combined the vessel shadow removal as well as the retinal tissue visibility improvement[21]. Additionally, we perform an intensity adjustment of the OCT image to a new specified range ($[0, 1] \rightarrow [0.2, 0.5]$) in order to facilitate the posterior process of segmentation of the subretinal fluid (Fig. 4(d)), next step of the proposed method.

2.3. Subretinal Fluid Segmentation

Given that the presence of the SRD edema includes dark positions, the corresponding columns have a fall of intensities, in their average values, as we can see in Fig. 5(a). Based on this principle, we established our strategy of the SRD edema extraction. In this way, a threshold is applied to the signal using the first quartile of the mean signal as reference. In the identified regions, we obtain their corresponding minimum values (Fig. 5(b)). These minimum

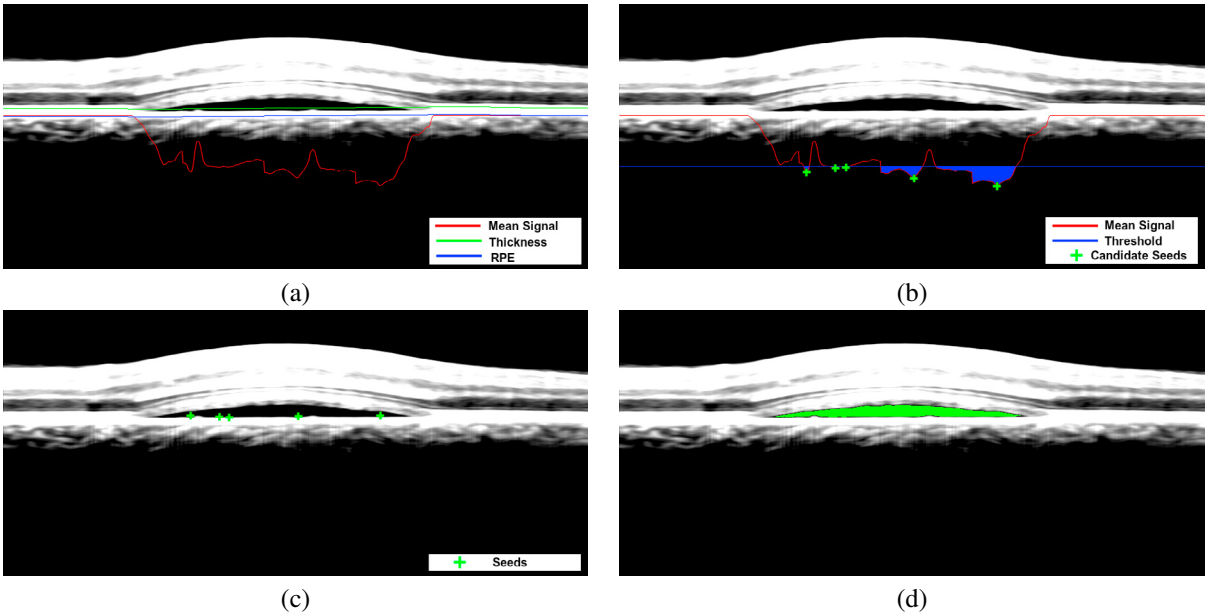

Fig. 5. Example of the subretinal fluid segmentation. (a) Signal representing the mean of intensity profiles in each column between the RPE retinal layer and a given thickness. (b) Fixed threshold estimated by the first quartile of the signal and the candidate seeds of the identified regions of the signal. (c) The seeds inside the subretinal fluid region. (d) The final result with the segmented subretinal fluid region.

values serve as seeds for the extraction of the entire target region. Therefore, the seeds are conveniently initialized in their corresponding columns in the mask (RPE/Thickness), where the thickness value was empirically estimated (Fig. 5(c)). If the intensity value of a seed is different from zero in this mask, it will be discarded as it does not belong to a fluid region. Finally, we used a method based on region growing to progressively add the neighboring pixels by intensity similarity (Fig. 5(d)), using a tolerance level of 0.01.

2.4. ELM Retinal Layer Segmentation

The SRD edema presence generates an abnormal change in the morphology of the retinal tissues that carries an elevation of the retinal layers that is associated to its detachment. This edema type is highly correlated with the integrity of the ELM retinal layer[22]. In this step, we perform a precise segmentation of the ELM layer for being characterized and facilitate the identification of cases where the accumulation of fluid is considered clinically significant (thickness values greater than $70\mu m \times 90\mu m$ along the x-y axis)[23]. To achieve this, we define a region of interest that is delimited between the ILM layer (previously segmented in the first step of the methodology) and the upper edge of the subretinal fluid (Fig. 6(a)). Then, we apply a combination of morphological operators and filters to detect the new region of interest that delimits the ELM layer to, therefore, significantly reduce the search space. In particular, in this stage a Gaussian difference (DoG) was used with a morphological erosion operator followed by a thresholding process (Fig. 6(b)). To facilitate the segmentation process, we project all the pixels of the new region of interest on a horizontal baseline (Fig. 6(c)). Then, we use a graph theory approach to segment the ELM layer, where the optimum connected paths from both sides of the image are found by dynamic programming (Fig. 6(d)). And finally, we recover this identification to the original image (Fig. 6(e)) to represent the segmented ELM layer over the input OCT image (Fig. 6(f)).

2.5. Neurosensorial Retinal Detachment Characterization

An automatic quantification and characterization of the SRD edema followed by an analysis of the consequent elevation and detachment of the retinal layers can help the doctors to make a more precise analysis and an early

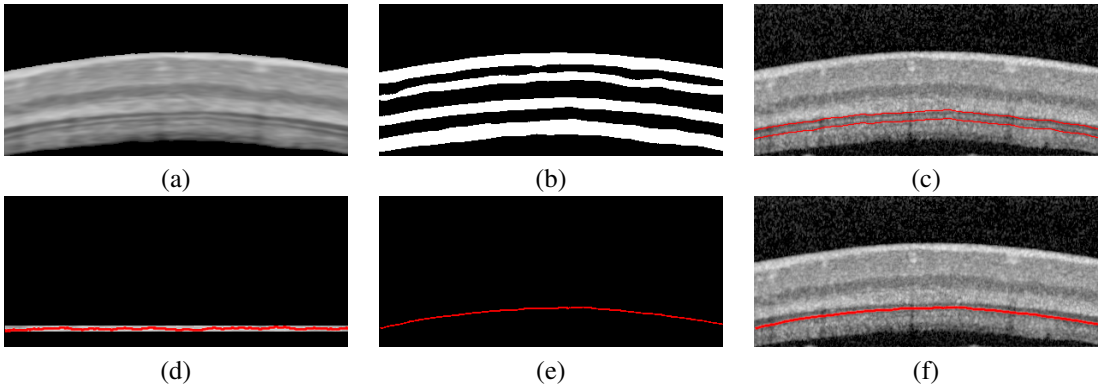

Fig. 6. Example of the ELM layer segmentation process. (a) The region of interest that is delimited between the ILM layer and the upper edge of the subretinal fluid in the preprocessing image. (b) The result of applying the combination of morphological operators. (c) The new region of interest that delimits the ELM layer in the original image. (d) Projection of all the pixels on a horizontal baseline and the ELM layer detected. (e) Projection of the ELM layer on the original baseline. (f) The final result with the segmented ELM layer.

diagnosis of various retinal and systemic pathologies[24]. In this way, we designed four visualization modules to provide means of intuitively characterizing the SRD edema in the OCT images. These visualization modules are: *subretinal fluid analysis*, *retinal layers visualization*, *retinal elevation and detachment representation* and *retinal thickness characterization*.

Regarding the subretinal fluid analysis module (Fig. 7(a)), six representative parameters were also calculated using the information that was obtained from the retinal layers and the subretinal fluid region: *number of the subretinal fluid*, *subretinal fluid x-axis*, *subretinal fluid y-axis*, *area of the retinal zone*, *area of the subretinal fluid* and *ratio between the area of the subretinal fluid and the area of the retinal zone*[25]. The retinal layers visualization module allows the analysis of the main retinal layers (ILM, RPE and ELM) and the contour of the area occupied by the SRD edema (Fig 7(b)). Regarding the retinal elevation and detachment representation module (Fig. 7(c)), we measure the thickness increase between the neurosensorial retina and the ELM layer. Finally, the retinal thickness characterization module allows the analysis of structural changes between the retinal layers (Fig. 7(d)). This measurement is commonly used by the experts to evaluate the severity of the SRD edema and the corresponding effect on the visual acuity[26].

3. Results and Discussion

The proposed method was tested using 38 OCT scans centered on the macula, captured from different patients that were diagnosed with the presence of the SRD edema. These images were taken with a Spectralis® OCT confocal scanning laser ophthalmoscope from Heidelberg Engineering, at a High-Resolution of 1024×480 pixels. The local ethics committee approved this study, which was conducted in accordance with the tenets of the Helsinki Declaration.

The initial dataset was manually labelled by an expert clinician. Hence, a total of 41 subretinal fluid regions and 4,364 points of the ELM retinal layers were manually extracted and categorized. Two representative experiments were designed to evaluate the performance of the proposed methodology, being statistically compared its results with the mentioned manual labelling of the expert clinician.

Regarding the subretinal fluid segmentation experiment, the performance of the method was evaluated using statistics that are commonly used in the state-of-the-art to measure the performance of computational proposals. Hence, sensitivity, specificity, Jaccard and Dice coefficients (Eqs. (1), (2), (3) & (4), respectively) were calculated for the quantitative validation of the results. These measures use as reference the true positives (TP), false positives (FP), true negatives (TN), and false negatives (FN).

$$\text{Sensitivity} = \frac{TP}{TP + FN} \tag{1}$$

$$\text{Specificity} = \frac{TN}{TN + FP} \tag{2}$$

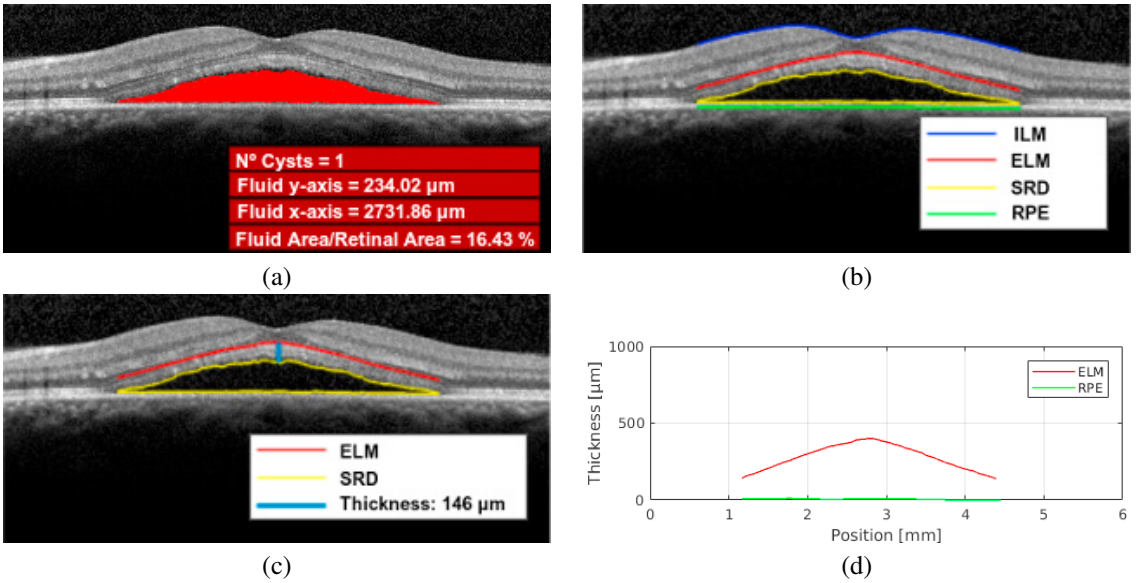

Fig. 7. Example of the neurosensorial retinal detachment characterization stage. (a) Subretinal fluid analysis module. (b) Retinal layers visualization module. (c) Retinal elevation and detachment representation module. (d) Retinal thickness characterization module.

$$\text{Jaccard} = \frac{TP}{TP + FP + FN} \tag{3}$$

$$\text{Dice} = \frac{2 \times TP}{2 \times TP + FP + FN} \tag{4}$$

Table 1 presents the results of the comparative analysis through sensitivity, specificity, Jaccard and Dice coefficients of the subretinal fluid segmentation. As we can see, the results provide a good balance between sensitivity and specificity (0.8930 and 0.9490, respectively). Jaccard and Dice coefficients also presented satisfactory results (0.7916 and 0.8353, respectively), demonstrating the suitability of the method not only in the identification of the SRD presence but also in the precise segmentation of its region. In Fig. 8, we can see illustrative examples of results where the proposed system detects and characterizes the subretinal fluids in these OCT images. Despite the satisfactory performance, some imperfections still remain in the obtained segmentations. Generally, these imperfections are mainly introduced by the projection of shadows derived by the vascularity or other artifacts that are present in the retinal layers. This situation generates patterns of intensities with an appearance similar to those of the subretinal fluid zone. Fig. 8, 2^{nd} row shows significative cases of overlapping of the clinical expert's annotations. Despite that few particular pixels, we can observe that our method presents a satisfactory segmentation performance with respect to the normal performance of the clinical specialist.

Table 1. Sensitivity, specificity, Jaccard and Dice coefficients in the calculation of the subretinal fluid segmentation.

Sensitivity	**Specificity**	**Jaccard**	**Dice**
0.8930	0.9490	0.7916	0.8353

Regarding the validation of the ELM retinal layer segmentation, the methodology was evaluated using the mean absolute error (MAE) and its standard deviation (SD) (Eqs. (5) & (6), respectively).

$$MAE = \frac{\sum_{i=1}^{n} |x_i - x|}{n} \tag{5}$$

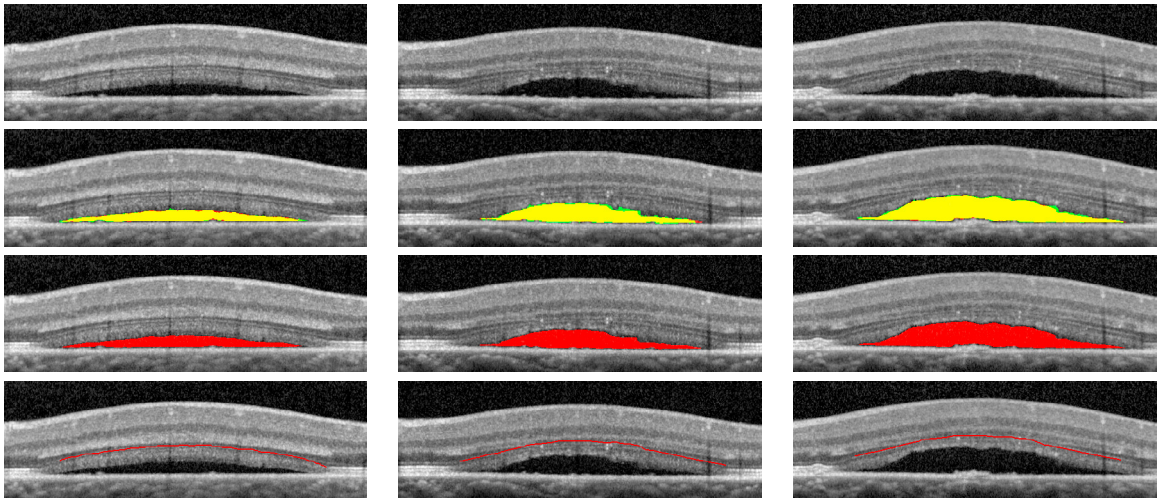

Fig. 8. Illustrative examples of OCT retinal images with the detection and characterization of SRD edemas. 1^{st} row, input images. 2^{nd} row, overlapping (yellow) of the clinical expert's annotations (green) and the resulting region of subretinal fluid segmentation (red). 3^{rd} row, results of the subretinal fluid segmentation method. 4^{th} row, results of the ELM retinal layer segmentation method.

$$SD = \sqrt{\frac{1}{n-1}\sum_{i=1}^{n}(x_i - \overline{x})^2} \tag{6}$$

Table 2 presents the results of this validation, including the mean absolute error (MAE) and the standard deviation (SD) in terms of pixels, micrometers and relative value index. The relative value index was calculated dividing each measurement by the height of the OCT image (1,920 μm). As we can see, satisfactory results were achieved, with a MAE of 0.0012 and a SD of 0.0014, both in terms of relative value index. As said, the ELM layer is detected as its elevation characteristics is a valuable source of information in cases where the accumulation of fluids was considered clinically significant (values greater than $70\mu m \times 90\mu m$ along the x-y axis)[23]. The abnormal elevation or detachment of the ELM retinal layer is only present in these specific cases. Fig. 8, 4^{th} row presents illustrative examples of results where the proposed system detects and characterizes the ELM retinal layer.

Table 2. Mean Absolute Error (MAE) and Standard Deviation (SD) in the calculation of the ELM retinal layer segmentation in terms of pixels, micrometers and relative value index.

Pixels (px)		Micrometers (μm)		Relative value index	
MAE	SD	MAE	SD	MAE	SD
0.60	0.68	2.39	2.76	0.0012	0.0014

As explained, to facilitate the clinical decision-making, four visualization modules (Fig. 7) were designed to provide means of intuitively characterizing the SRD edema in the OCT images. These modules also provide different representative biomarkers that allow the clinical specialists to make a more precise analysis and characterization of a relevant disease as is the presence of the SRD edema.

4. Conclusions

Blindness and visual impairment derived by the ME disease are important public health problems, particularly in the working-age population of developed countries. An accurate detection and subsequent characterization of the SRD edema presence, a specific clinical type of ME, is crucial for the early diagnosis and appropriate treatment to reduce the associated costs and improve the patient's quality of life.

In this paper, a new method is proposed for the automatic identification and characterization of the SRD edema presence in OCT images. To achieve this, the subretinal fluids and the ELM retinal layer are extracted, analysed and characterized. Using these extractions, the system provides different intuitive visualization modules including relevant representative biomarkers, facilitating the doctor's work in the diagnosis and treatment processes associated with the ME disease. The robustness and accuracy of the proposed methodology were evaluated using a representative set of OCT images with the presence of the SRD edema. The images were labelled by an expert clinician, groundtruth that was used to validate the proposed method, obtaining satisfactory results.

In future works, we plan to improve the methodology to reinforce the accuracy of the obtained results. In addition, a more complete validation is planned using a large dataset of retinal OCT images to consolidate the reached conclusions.

Acknowledgements

This work is supported by the Instituto de Salud Carlos III, Government of Spain and FEDER funds of the European Union through the PI14/02161 and the DTS15/00153 research projects and by the Ministerio de Economía y Competitividad, Government of Spain through the DPI2015-69948-R research project. Also, this work has received financial support from the European Union (European Regional Development Fund - ERDF) and the Xunta de Galicia, Centro singular de investigación de Galicia accreditation 2016-2019, Ref. ED431G/01; and Grupos de Referencia Competitiva, Ref. ED431C 2016-047.

References

1. World Health Organization. Vision impairment and blindness. 2017; Available at `http://www.who.int/mediacentre/factsheets/fs282/en/`
2. Moura J, Novo J, Charlón P, Barreira N, Ortega M. Enhanced visualization of the retinal vasculature using depth information in OCT. *Medical and biological engineering and computing.* 2017; **55**(12):2209-25.
3. Deshpande A, Harris-Hayes M, Schootman M. Epidemiology of diabetes and diabetes-related complications. *Physical Therapy.* 2008; **88**(11):1254-64.
4. Cheung N, Mitchell P, Wong T. Diabetic Retinopathy. *The Lancet Global Health.* 2010; **376**(9735):12436.
5. Browning D, Altaweel M, Bressler N, Bressler S, Scott I. Diabetic macular edema: what is focal and what is diffuse? *American Journal of Ophthalmology.* 2008; **146**(5):649-55.
6. Moura J, Novo J, Rouco J, Penedo M, Ortega M. Automatic Identification of Intraretinal Cystoid Regions in Optical Coherence Tomography. *Artificial Intelligence in Medicine in Europe.* 2017; 305-315.
7. Xiao H, Liu X, Guo X. Macular edema with serous retinal detachment post-phacoemulsification followed by spectral domain Optical Coherence Tomography: a report of two cases. *BMC Research notes.* 2015; **8**(1):647.
8. Huang D, Swanson E, Lin C, Schuman J, Stinson W, Chang W, Hee M, Flotte T, Gregory K, Puliafito C. Optical Coherence Tomography. *Science*. 1991; **254**(5035):1178-81.
9. Otani T, Kishi S, Maruyama Y. Patterns of diabetic macular edema with Optical Coherence Tomography. *American journal of ophthalmology.* 1999; **127**(6):688-93.
10. Panozzo G, Parolini B, Gusson E, Mercanti A, Pinackatt S, Bertoldo G, Pignatto S. Diabetic macular edema: an OCT-based classification. *InSeminars in ophthalmology.* 2004; **19**(1-2):13-20.
11. Baamonde S, de Moura J, Novo J, Ortega M. Automatic Detection of Epiretinal Membrane in OCT Images by Means of Local Luminosity Patterns. *InInternational Work-Conference on Artificial Neural Networks.* 2017; 222-235.
12. Marmor M. On the cause of serous detachments and acute central serous chorioretinopathy. *British journal of ophthalmology.* 1997; **81**(10):812-3.
13. Lee S, Stetson P, RuizGarcia H, Heussen F, Sadda S. Automated characterization of pigment epithelial detachment by Optical Coherence Tomography. *Investigative ophthalmology and visual science.* 2012; **53**(1):164-70.
14. Hassan B, Raja G, Hassan T, Akram M. Structure tensor based automated detection of macular edema and central serous retinopathy using Optical Coherence Tomography images. *JOSA A.* 2016; **33**(4):455-63.
15. Wu M, Fan W, Chen Q, Du Z, Li X, Yuan S, Park H. Three-dimensional continuous max flow optimization-based serous retinal detachment segmentation in SD-OCT for central serous chorioretinopathy. *Biomedical optics express.* 2017; **8**(9):4257-74.
16. Schlegl T, Waldstein SM, Bogunovic H, Endstraßer F, Sadeghipour A, Philip A, Podkowinski D, Gerendas B, Langs G, Schmidt-Erfurth U. Fully Automated Detection and Quantification of Macular Fluid in OCT Using Deep Learning. *Ophthalmology.* 2017.
17. Samagaio G, Estévez A, de Moura J, Novo J, Ortega M, Fernández M, Automatic Identification of Macular Edema in Optical Coherence Tomography Images, *VISIGRAPP*, 2018; **1**(4):533-540.
18. Chiu S, Li X, Nicholas P, Toth C, Izatt J, Farsiu S. Automatic segmentation of seven retinal layers in SDOCT images congruent with expert manual segmentation. *Optics express.* 2010; **18**(18):19413-28.
19. Dijkstra E. A note on two problems in connexion with graphs. *Numerische mathematik.* 1959; **1**(1):269-71.

20. Kroon D, Slump C, Maal T. Optimized anisotropic rotational invariant diffusion scheme on cone-beam CT. *International Conference on Medical Image Computing and Computer-Assisted Intervention* 2010; 221-228.
21. Mari J, Strouthidis N, Park S, Girard M. Enhancement of lamina cribrosa visibility in Optical Coherence Tomography images using adaptive compensation. *Investigative ophthalmology and visual science.* 2013; **54**(3):2238-47.
22. Lin H, Yeh P, Huang J. Optical Coherence Tomography study of foveal microstructure after successful retinal detachment surgery. *Taiwan Journal of Ophthalmology.* 2013; **3**(3):103-7.
23. Gelfand J, Nolan R, Schwartz D, Graves J, Green A. Microcystic macular oedema in multiple sclerosis is associated with disease severity. *Brain.* 2012; **135**(6):1786-93.
24. Gerendas B, Kroisamer J, Buehl W, RezarDreindl S, Eibenberger K, Pablik E, SchmidtErfurth U, Sacu S. Correlation between morphological characteristics in SpectralDomainOptical Coherence Tomography, different functional tests and a patient's subjective handicap in acute central serous chorioretinopathy. *Acta ophthalmologica.* 2018.
25. Baek J, Park Y. Optical density ratio in the subretinal fluid: differentiating chronic central serous chorioretinopathy and polypodial choroidal vasculopathy. *American journal of ophthalmology.* 2015; **159**(2):386-92.
26. Noma H, Funatsu H, Mimura T, Shimada K. Visual function and serous retinal detachment in patients with branch retinal vein occlusion and macular edema: a case series. *BMC ophthalmology.* 2011; **11**(1):29.